Structural Engineering and Mechanics, *Vol. 65, No. 2 (2018) 155-162*
DOI: https://doi.org/10.12989/sem.2018.65.2.155

On strain measurement of smart GFRP bars with built-in fiber Bragg grating sensor

Minkwan Ju[1a], Kyoungsoo Park[1b], Doyoung Moon*[2b], Cheolwoo Park[3c] and Jongsung Sim[4c]

[1]*Department of Civil and Environmental Engineering, Yonsei University, 50 Yonsei-ro, Seodaemun-gu, Seoul, 03722, Republic of Korea*
[2]*Department of Civil Engineering, Kyungsung University, 309 Sooyoung-ro, Nam-gu, Busan, 48434, Republic of Korea*
[3]*Department of Civil Engineering, Kangwon National University, 1 Joongang-ro, Samcheok-si, Kangwon, 25913, Republic of Korea*
[4]*Department of Civil and Environmental Engineering, Hanyang University, 55 Hanyangdaehak-ro, Sangnok-gu, Ansan, Gyeonggi-do,15588, Republic of Korea*

(Received December 15, 2017, Revised December 17, 2017, Accepted December 18, 2017)

Abstract. A smart glass fiber reinforced polymer (SMFRP) reinforcing bar with a fiber Bragg grating (FBG) sensor was fabricated using a pultrusion technique, while ribs were formed to improve bonding between concrete and SMFRP. Then, strain of SMFRP bars were measured for a uniaxial tension test of an SMFRP bar, and a four-point bending test of concrete beams reinforced with SMFRP bars. The results of a uniaxial tension test illustrate that the strain obtained from an FBG sensor agrees well with that obtained from electrical resistance strain gauge (ERSG). Additionally, concrete beams reinforced with SMFRP bars were fabricated, and actual flexural test were performed while the strain of with an FBG sensor was compared with that of ERSG. The experimental results demonstrate that SMFRP bars can be used as reinforcement of concrete member while providing deformation information. Furthermore, SMFRP bars may provide stronger durability and smart monitoring to reinforced concrete members under corrosive environments during a service life.

Keywords: SMFRP bar; fiber Bragg grating (FBG) sensor; strain, reinforced concrete; four point bending test

1. Introduction

Fiber reinforced polymer (FRP) bars have been commonly considered as a substitute for a conventional steel bar for higher durability of reinforced concrete (RC) structures. Its high strength-to-weight ratio, non-corrosive characteristic, and easy handling in construction are main advantages of FRP bars for infrastructure. Previous experimental investigations associated with bending, shear, compression and impact behaviors of FRP reinforced concrete members demonstrated the validity for the potential use of FRP bars as a new reinforcement (Maranan *et al.* 2015, Thomas and Ramadass 2015, Ali *et al.* 2013, Ali *et al.* 2016, Refai *et al.* 2015, Goldston *et al.* 2016). The development of the design specifications (ACI 440.1R-15 2015, CSA S806-12 2012) have encouraged the construction industry to use FRP bars. The application of FRP bars in reinforced concrete have been widely considered such as concrete slab for shear (Abdul-Salam *et al.* 2016), RC columns (Bai *et al.* 2017), and others.

However, because of a low modulus of elasticity for FRP bars, serviceability requirements, such as crack width or allowable deflection of a structure, are critical, especially for a long-term behaviors. As a result, FRP reinforced concrete structures suffer from an excessive deflection or wider crack width during their service life. In this case, the design of FRP reinforced concrete structures is generally governed by their serviceability limit state rather than that of the ultimate limit state. Accordingly, the deformation of FRP bars should be monitored to check whether a structure excesses the serviceability limit during its service life. A research related with improving the lower flexural stiffness of FRP reinforced concrete structures by using the encased steel composite is introduced (Kara 2016).

A simple method to measure deformation variations is to use an electrical resistance strain gauge (ERSG). However, for a long-term monitoring of strain, the use of ERSG may be limited because of the bonding between FRP bar surface and ERSG, and an electromagnetic interference (EMI) under a high-voltage electric power feeding system (Chung and Kang 2008, Edward 2000). Additionally, a vibrating wire strain gauge, which is one of the general use for the strain measurement, also demonstrated that the measured strain is sensitive under the EMI environment (Tan *et al.* 2008).

Alternatively, a fiber optic Bragg grating (FBG) sensor, which is one type of a fiber optic sensor (FOS), has been widely employed for the strain measurement in structural health monitoring of civil infrastructure. Note that an FBG sensor is a small size, light weight, and EMI–free, and can provide long-range data communication in a wide area network (WAN) system (Moyo *et al.* 2005). For example, FBG sensors were used in concrete structures to quantify strain (Tian *et al.* 2015, Benmokrane *et al.* 2006, Rodrigues *et al.* 2010), corrosion cracking of concrete (Mao *et al.*

*Corresponding author, Associate Professor
E-mail: dymoon@ks.ac.kr
[a]Research Professor
[b]Associate Professor
[c]Professor

ISSN: 1225-4568 (Print), 1598-6217 (Online)

2016), fatigue and dynamic performance of cable tension (De Baere *et al.* 2009, Li *et al.* 2012), long-term behaviors of concrete bridges (Huang and Newhook 2008), performance of a marine composite structural joint (Li *et al.* 2006), and high strain of a nuclear power vessel (Perrya *et al.* 2014).

Furthermore, a FBG sensor was embedded in fiber reinforced polymer (FRP) to measure strain and detect damage of externally bonded FRP composites (e.g., sheets, plates, and laminates). For example, an embedded FBG sensor was employed to monitor internal defects of a sandwich composite member with glass fiber reinforced polymer (GFRP) (Dawood *et al.* 2007, Jensen *et al.* 2000), damage of a glass fiber laminate (Lau *et al.* 2001), buckling of carbon fiber reinforced polymer (CFRP) stiffened panels (Takeda *et al.* 2012), peeling phenomenon of a CFRP sheet (Zhao *et al.* 2009), pultruded FRP reinforcements (Kalamkarov *et al.* 2000), and CFRP laminates under the uniaxial tensile cyclic loading (Shin and Chiang, 2006). Additionally, Lu and Xie (2007) performed a bending test with an RC specimen strengthened with a carbon fiber reinforced polymer (CFRP) sheet, and the test results illustrated that the strain of an FBG sensor matched well with a theoretically calculated strain. Tsuda and Lee (2007) employed an embedded FBG sensor for an impact test, and the measured strain with an FBG sensor captured sudden variations of tensile and compressive behaviors according to time. Huang *et al.* (2013) and Li *et al.* (2011) fabricated a self-sensing FRP anchor rod with built-in an FBG sensor to measure strain of bridge stay cables.

In this context, the present study proposes to embed an FBG sensor to GFRP bars, named as a smart FRP bar with an FBG sensor (SMFRP bar), and to use SMFRP bars as reinforcement of concrete members. An SMFRP bars are fabricated using a pultrusion process, while surface ribs are formed by employing high temperature and pressure. To validate the accuracy of an FBG sensor, a uniaxial tension test of an SMFRP bar is performed. The results demonstrate that the strain of an FBG sensor matches well with the strain of electrical resistance strain gauges (ERSG). For a bending test of concrete beams reinforced with SMFRP bars, a cross section is designed in accordance with ACI 440 1R-15, while electrical resistance strain gauges (ERSG) were also placed on the surface of SMFRP bars for the comparison purpose. The strain obtained from ERSG is compared with the strain from an FBG sensor, while the sources of the differences between ERSG and an FBG sensor are discussed. Finally, the results demonstrate that the use of SMFRP bars is possible to monitor structural behaviors.

2. Fiber optical SMFRP bar

2.1 FBG sensor

In a FBG sensor, strain is measured by calculating the change in a signal reflected from fiber Bragg gratings when a fiber core elongates. A grating, which acts essentially as a wavelength-selective mirror, must be firstly written in the core of an optical fiber, as shown in Fig. 1. The grating is written by exposing an optical fiber to an interfering pair of strong ultraviolet (UV) signals. When input spectrum is transmitted along an optical fiber, the intensity (I) of reflected spectrum changes due to the elongation of an optical fiber. Then, strain is obtained from a reflected signal processor. The schematic illustration is shown in Fig. 1. Fiber optic Bragg grating sensor response arises from two sources; change in a pitch length (Λ) of the grating and the effective index of fundamental mode of optical fiber (n_{eff}). Then, the wavelength (λ_B) of the reflected spectrum band is defined with the Bragg condition, i.e.,

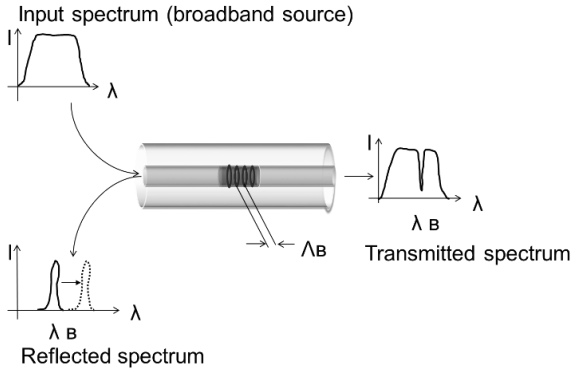

Fig. 1 Schematic illustration of FBG in strain measurement

$$\lambda_{\mathrm{B}} = 2n_{\mathrm{eff}}\Lambda \tag{1}$$

When the pitch length increases, the Bragg wavelength (λ_B) changes. Then, due to the change of the Bragg wavelength ($\Delta\lambda_B$), the corresponding strain is given by

$$\varepsilon = \frac{\Delta\lambda_B}{\lambda_B}\frac{1}{(1-p_e)} \tag{2}$$

where p_e is the strain optic coefficient, which can be obtained from

$$p_e = \frac{{n_{\mathrm{eff}}}^2}{2}[p_{12} - \nu(p_{11} + p_{12})] \tag{3}$$

In this study, the strain optic constant, p_{11} and p_{12}, are 0.113 and 0.252, respectively, with the Poisson's ratio of the optical fiber of 0.16. The average refractive index (n_{eff}) is 1.482 (Yin *et al.* 2008). Then, the strain shift of the FBG sensor is 833 με per a unit wavelength (1 nm).

2.2 Manufacturing of SMFRP bar

To manufacture an SMFRP bar, a pultrusion process is employed, as illustrated in Fig. 2. An SMFRP bar consists of an FBG sensor, 65.0% of E-glass fiber (by weight) and a epoxy resin. While polymer impregnated glass fibers are proceeded to form a glass fiber core, an optical fiber with an FBG sensor is placed at the center of a glass fiber core. Then, after applying a longitudinal force to a fiber core for the fiber alignment, a fiber core is pressed for 20 minutes under the thermal curing condition of 170°C (Fig. 3). Note that ribs are formed on the surface of an SMFRP bar to enhance bonding performances without sustaining any rupture damage. The nominal diameter of an SMFRP specimen was 9.53 mm obtained by the design diagram.

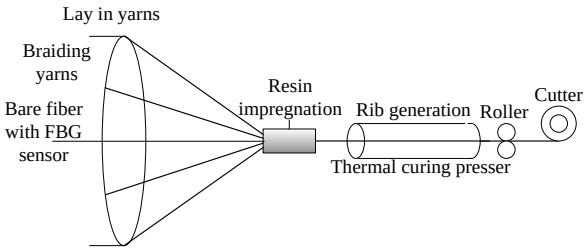

Fig. 2 A schematic example of the pultrusion process for SMFRP bar

(a) Pultrusion bed

(b) Pultrusion bed and polymer impregnation

(c) Tentative formation of glass fiber core

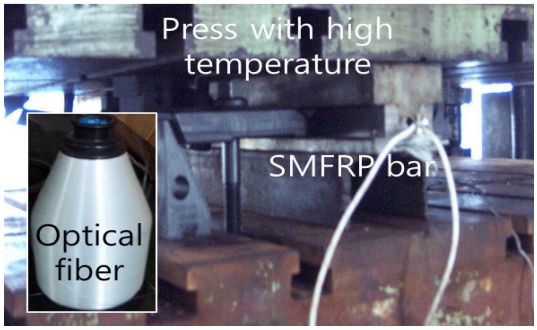

(d) Thermosetting and completion

Fig. 3 A fabrication steps of SMFRP bar

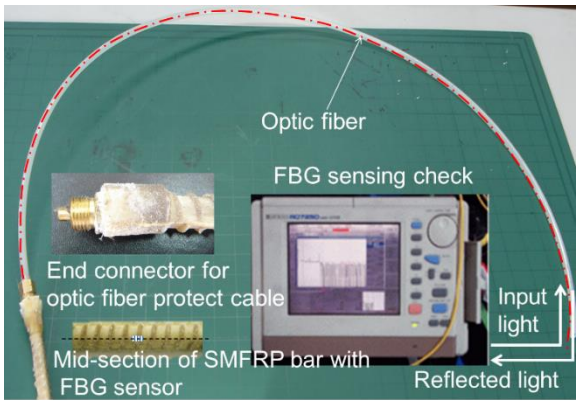

Fig. 4 FBG sensing check of SMFRP bar

Table 1 Material properties of E-glass fiber and polymer

	Tensile strength (MPa)	Modulus of elasticity (GPa)	Elongation (%)
Fiber (E-Glass)	1,840	75	1.3
Polymer Matrix (epoxy)	73.8	2.73	5

Fabrication details and experimental results of bonding behaviors of an FRP bar with ribs can be found in literature (Ju and Oh 2015). Finally, the input and reflected spectrums are checked, which completes the fabrication of an SMFRP bar (Fig. 4). The mechanical properties of an SMFRP bar is summarized in Table 1.

3. Uniaxial tensile test of an SMFRP bar

To validate the accuracy of the FBG sensor in an SMFRP bar, the uniaxial tensile test of an SMFRP bar was performed. At the ends of the SMFRP bar, a wedge-type anchor was fabricated using epoxy, which was gripped by a steel jig (see Fig. 5). On the surface of the SMFRP bar, an ERSG is attached for the comparison purpose. Then, the SMFRP specimen is elongated using a universal testing machine (UTM) with the loading capacity of 2,000 kN, and the loading rate of 17.8 kN/min.

Fig. 6 demonstrates the stress and strain relationship for the SMFRP bar. The strain obtained from the FBG sensor agrees well with the strain obtained from ERSG, which confirms the accuracy of the FBG sensor. Whereas, the tension test was terminated at the applied load of 357 MPa because of anchorage failure. The anchorage failure may be resulted from partial fracture of the filled resin inside the steel tube. Note that Ju *et al.* (2016) performed a uniaxial tension test of a FRP bar which has same material property with SMFRP bar in compliance with ACI 440.3R-04 (2004) average tensile strength was measured as equal to 841.0±23.6 MPa and the design tensile strength of 539.1MPa (Ju and Oh 2015). Accordingly, in spite of premature failure of SMFRP bar, the tested tensile stress level was measured as equal to 66.2% to the design tensile stress. These experimental results might explain that the strain monitoring with an SMFRP bar is able to provide sufficiently stable measurement around the service load state as well as the ultimate load state.

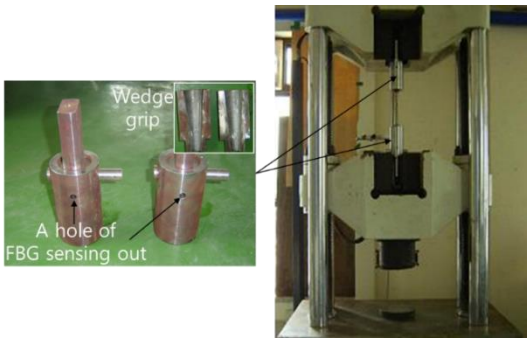

Fig. 5 Uniaxial tensile test of SMFRP bar

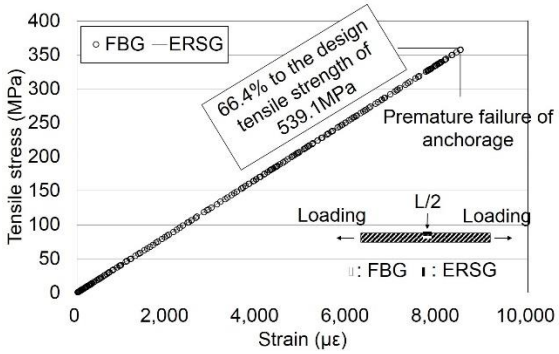

Fig. 6 Tensile strain measurement between FBG and ERSG sensor

4. Flexural test of concrete beams reinforced with SMFRP bars

To demonstrate the applicability of the SMFRP bars to concrete structures, flexural tests are performed in this study. The design of a concrete beam reinforced with SMFRP bars is based on ACI 440 1R-15 (2015) the strain measured from the SMFRP bar is compared with the strain obtained from ERSG.

4.1 Design of a concrete beam

In a FBG sensor, two types of concrete beams are preared, i.e., one reinforced with SMFRP bars, and the oher reinforced with steel bars. For a beam reinforced with SMFRP bars, a cross section is designed so that the beam leads to the failure of SMFRP rupture, although the design standards (ACI 440.1R-15) generally recommends an over-reinforced section for an GFRP design. This is because an under reinforced section can lead to larger strain during a flexural test. Accordingly, the strain accordance is investigated when FBG strain measurement is compared with that of ERSG.

In this study, the cross section of the concrete beam was selected as 180 × 230 mm, and three SMFRP bars were placed, as shown in Fig. 7. The vertical stirrups were placed with steel bars. The elastic modulus and the yield strength of steel bars are 200 GPa and 30 MPa, respectively. The spacing of the stirrups was 100 mm, and No. 3 bars were utilized. The elastic modulus of concrete (E_c) and the compressive strength of concrete (f_c') were 25.5 GPa, and 27 MPa, respectively. The FRP reinforcement ratio (ρ_f) was

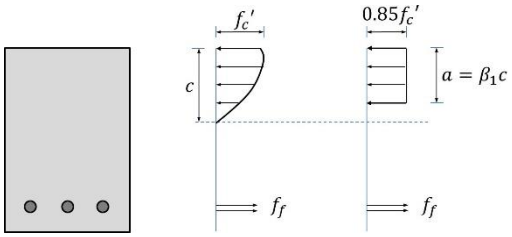

Fig. 7 Failure stress diagram of SMF-B specimen (governed by GFRP rupture)

0.0064, while the balanced reinforcement ratio of the SMFRP section is 0.0069. elastic modulus of SMFRP bar (E_f)is the design or guaranteed modulus of 42.1 GPa (ACI 440 1R-15). The applied stress in an SMFRP bar (f_f) can be obtained as equal to the design tensile strength of an SMFRP bar (f_f) of 539.1 MPa from

$$f_f = \left(\sqrt{\frac{\left(E_f \varepsilon_{cu}\right)^2}{4} + \frac{0.85\beta_1 f_c'}{\rho_f} E_f \varepsilon_{cu}} - 0.5 E_f \varepsilon_{cu} \right) \leq f_{fu} \quad (4)$$

The typical equilibrium of forces and strain compatibility is illustrated in Fig. 8. Additionally, the ultimate strain of concrete (ε_{cu}) is selected as 0.003 with β_1 of 0.85. d and a are the depth of a beam, and the depth of an equivalent rectangular stress block, respectively. Then, the estimated nominal moment for the section is 19.9 kN-m. When ρ_f is lower than the balanced FRP reinforcement ratio, the nominal moment (M_n) is evaluated as

$$M_n = A_f f_f \left(d - \frac{a}{2} \right) \quad (5)$$

For the design of a concrete beam with steel bars, the cross section and the reinforcement ratio are the same as those of the beam with the SMFRP bars, which leads to the nominal moment of 11.4 kN-m. Additionally, the balanced reinforcement ratio was 0.0434. Then, three No. 3 steel bars were placed at the bottom, while vertical stirrups were provided, as in the concrete beam reinforced with SMFRP bars.

4.2 Test setup

For flexural tests of concrete beams, the length of beams was 2,000 mm with the span of 1,600 mm. Three concrete beams reinforced with SMFRP bars (SMF-B) were fabricated, while two concrete beams reinforced with steel bars (ST-B) was prepared. The FBG sensor was placed at the center and quarter points of the span, as illustrated in Fig. 8. For comparison purposes, two ERSGs with 5 mm gauge length were bonded on the surface of SMFRP bar along the same longitudinal location where the FBG sensor was embedded. Fig. 9 shows the schematic view of a concrete beam (SMF-B) reinforced with an SMFRP. Then, four points bending test was conducted using a hydraulic loading machine (MTS actuator) with the capacity of 250 kN. The span to depth ratio was designed as 3.7, which was subjected to pure bending.

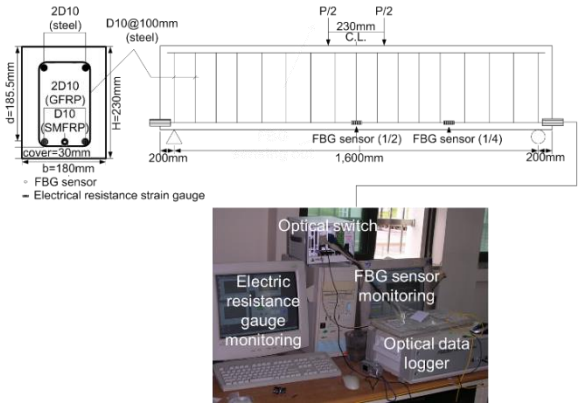

Fig. 8 Flexural loading test and strain monitoring by FBG and ERSG

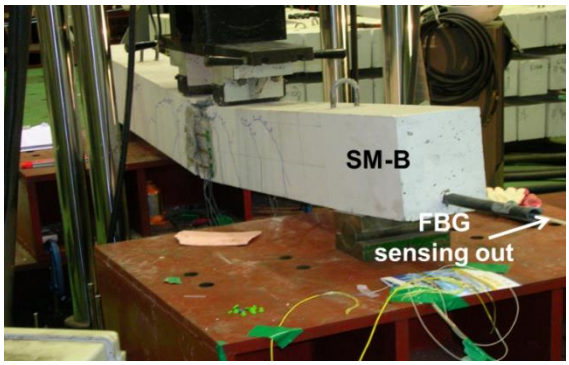

Fig. 9 Flexural failure of SMFRP bar reinforced concrete beam

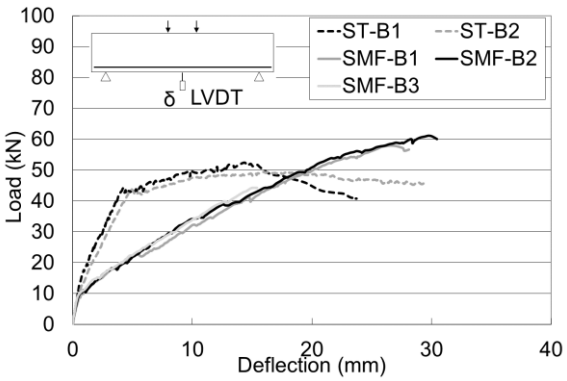

Fig. 10 Load-deflection curves of the flexural tests

5. Results and discussion

Flexural failure and crack patterns of a tested beam reinforced with SMFRP bars is illustrated in Fig. 9. Table 2 summarized the ultimate loads and deflections by tested and calculated from beam theory. The average ultimate load and maximum moment of two test specimens (SMF-B1 and SMF-B2) is 59.6 kN and 20.4 kN-m, respectively. Note that SMF-B3 is not included for the average, because the SMF-B3 specimen demonstrates an unexpected early failure of concrete in a compressive zone. The ratio of the tested maximum moment to the nominal moment is 1.03, which shows the good agreement between the test results and the flexural design.

Table 2 Flexural test results of the beams reinforced with SMFRP bars and steel bars

		Ultimate load (kN)		Deflection (mm)		Max. moment (kN-m)	
		Test	Avg.	Test	Avg.	Test	Avg.
Reinforced with SMFRP bars	SMF-B1	57.9	59.6*	26.8	28.3*	19.8	20.4*
	SMF-B2	61.2		29.7		21.0	
	SMF-B3	44.2					
Reinforced with steel bars	ST-B1	52.5	51.0	14.2	15.1	18.0	11.4
	ST-B2	49.4		16.0		16.9	

*Not including SMF-B3

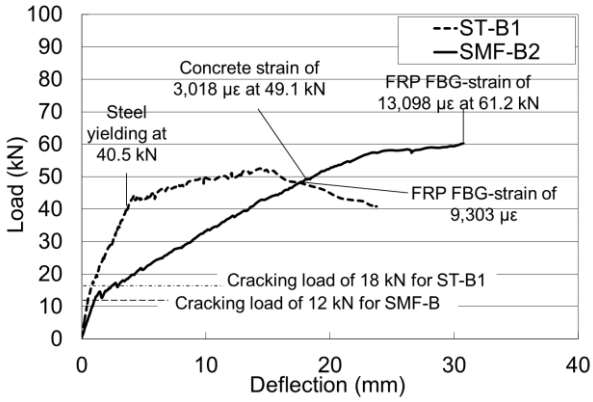

Fig. 11 Comparison between the ST-B1 and the SMF-B2 specimen

Fig. 10 illustrates the relationships between the applied load and deflection of the SMFRP reinforced concrete beams and the steel reinforced beams. For the SMFRP reinforced beams, each test results displayed similar load-deflection curves including cracking loads. After reaching the ultimate load, SMFRP bars were ruptured, and then concrete crushing failure occurred, as expected in design of the cross section. For the steel reinforced beam, after yielding of steels bars around 40.5 kN, the beams reached the maximum moment, which demonstrates the under-reinforced section behavior.

For the comparison between the SMFRP reinforced beams and the steel bar reinforced beams, the SMF-B2 and ST-B1 specimens are representatively selected. For the SMF-B2 specimen, the strain at the ultimate state was 13,098 $\mu\varepsilon$, as shown in Fig. 11. The flexural stiffness of the SMF-B2 specimen was noticeably lower than that of the ST-B specimen, especially after cracking load. This was because SMFRP bars had less modulus of elasticity than that of steel bars. The ultimate load carrying capacity of the SMF-B specimen was 16.9% higher than that of the ST-B specimen owing to the high tensile strength of the SMFRP bars.

Additionally, for the SMFRP reinforced beams, the strain obtained from the FBG sensor was compared with the strain obtained from the ERSG. Note that the SMFRP reinforced beams demonstrated relatively large deflections, and thus the larger longitudinal deformation and strain were expected. Fig. 11 showed the vertical load versus strain curves obtained from the ERSG and the FBG sensors. In

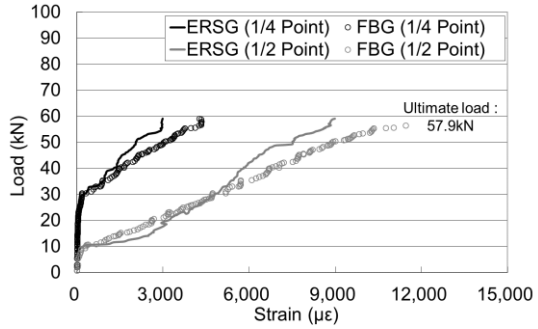

(a) SMF-B1

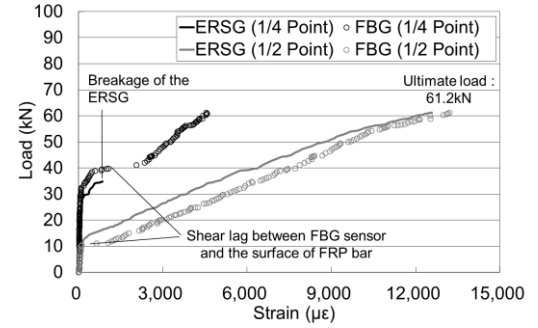

(b) SMF-B2

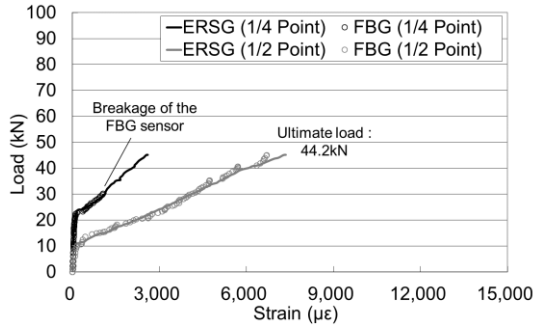

(c) SMF-B3

Fig. 12 Comparison between the strain obtained from the FBG sensors and the strain obtained from ERSG: (a) SMF-B1, (b) SMF-B2, (c) SMF-B3

general, the ERSG and the FBG sensor provided similar trends of strain variations. However, the disagreement between the strain of ERSG and the strain of the FBG sensor were observed in the flexural tests. Such differences may be resulted from the following reasons. First, one may consider a fabrication error associated with the alignment of the embedded FBG sensor during the pultrusion process, and thus a less accurate measurement may be expected if an FBG sensor is not parallel with an SMFRP bar. Next, the location of an FBG section may be different from the location of an ERSG. Then, if a crack is initiated around an FBG sensor, but not around ERSG, relatively larger strain can be measured from an FBG sensor than ERSG. This could explain that the test results showed that the strain measurements obtained from the FBG sensor were higher than those from the ERSG approaching to the ultimate loading (see Fig. 12(a)). Kalamkarov *et al.* (2000) analyzed the discrepancy because the shear lag existed between the FBG sensor core and the surface of the SMFRP bar, and it might contribute to the discrepancy Besides, they monitored the strain embedded in the smooth FRP bar until 2,500 $\mu\varepsilon$. The deformed FRP bar in this study could have much longer range of strain reading due to the enhanced bond capacity. As a result, this study found that the strain measurement of the FBG sensor was quite valid for investigating structural behaviors for flexural failure.

5. Conclusions

This study investigates the validity of strain monitoring of SMFRP bars by comparing the strain obtained from ERSG to that from an FBG sensor. The key findings of the present study are summarized as follows:

• Strain measurements under a tensile test of an SMFRP bar showed the good agreement between an FBG sensor and ERSG, although anchorage failure was observed before approaching the ultimate load. Then, the fabricated SMFRP bars can effectively provide accurate strain when they are used as reinforcement of concrete structures.

• For a flexural behavior of a concrete beam reinforced with the SMFRP bars, the longitudinal strain of the SMFRP bars was measured. However, the strain from an FBG sensor was slightly different from the strain of ERSG. Because the strain behavior varies along the longitudinal direction of SMFRP bar under flexure, the location of strain measurement was important for comparison of the strains from an ERSG and an FBG sensor. The embedded FBG sensor could have a reliable strain measurement even where a crack occurs. The installation position of the FBG sensor should be improved to be placed at the center of the SMFRP bar as exactly as possible. There was a result of the beam test which showed the perfect measurement between the ERSG and the FBG sensor so that the feasibility of the strain monitoring of the SMFRP bar was verified.

• SMFRP bars can devote to make highly durable reinforced concrete structures as well as the smart monitoring of strain during a serve life of a structure. For further study, multi-functional techniques, e.g., measuring strain and temperature, can be utilized for concrete members reinforced with SMFRP bars, while being integrated with informative communication technologies (ICT).

Acknowledgments

This research was supported by a grant(13SCIPA01) from Smart Civil Infrastructure Research Program funded by Ministry of Land, Infrastructure and Transport(MOLIT) of Korea government and Korea Agency for Infrastructure Technology Advancement(KAIA) and Basic Science Research Program through the National Research Foundation of Korea (NRF) funded by the Ministry of Education (#2016R1D1A1B03934809).

References

Abdul-Salam, B., Farghaly, A.S. and Benmokrane, B. (2016), "Mechanisms of shear resistance of one-way concrete slabs

reinforced with FRP bars", *Constr. Build. Mater.*, **127**, 959-970.
ACI Committee 440 (2015), *Guide for the Design and Construction of Concrete Reinforced with FRP Bars (ACI 440.1R-15)*, American Concrete Institute, Farmington Hills, Michigan, U.S.A.
ACI Committee 440 (2004), *Guide Test Methods for Fiber-Reinforced Polymers (FRPs) for Reinforcing or Strengthening Concrete Structures (ACI 440.3R-04)*, American Concrete Institute, Farmington Hills, Michigan, U.S.A.
Ali, A.H., Mohamed, H.M. and Benmokrane, B. (2013), "Shear resistance of circular concrete members reinforced with FRP bars: code predictions and numerical analysis", *Proceedings of the CSCE Annual Conference on Canadian Society for Civil Engineering (CSCE)*, Montreal, Canada.
Ali, A.H., Mohamed, H.M. and Benmokrane, B. (2016), "Strength and behavior of circular FRP reinforced concrete sections without web reinforcement in shear", *J. Struct. Eng.*, **143**(3).
Bai, Y.L., Dai, J.G. and Teng, J.G. (2017), "Buckling of steel reinforcing bars in FRP-confined RC columns: An experimental study", *Constr. Build. Mater.*, **140**, 403-415.
Benmokrane, B., Debaiky, A., El-Ragaby, A., Roy, R., El-Gamal, S. and El-Salakawy, E. (2006), "Laboratory and field performance of FOS sensors in static and dynamic strain monitoring in concrete bridge decks", *Proceedings of SPIE 2006-Nondestructive Evaluation and Health Monitoring of Aerospace Materials*, Composites, and Civil Infrastructure, San Diego, California, U.S.A.
CAN/CSA S806-12 (2012), *Design and Construction of Building Structures with Fibre-Reinforced Polymers, Canadian Standards Association/National Standard of Canada*, Ontario, Canada.
Chung, W. and Kang, D. (2008), "Full-scale test of a concrete box girder using FBG sensing system", *Eng. Struct.*, **30**(3), 643-652.
Dawood, T.A., Shenoi, R.A. and Sahin, M. (2007), "A procedure to embed fibre Bragg grating strain sensors into GFRP sandwich structures", *Compos. Part A: Appl. Sci. Manufact.*, **38**, 217-226.
De Baere, I., Luychx, G., Voet, E., Van Paepegem, W. and Degrieck, J. (2009), "On the feasibility of optical fibre sensors for strain monitoring in thermoplastic composites under fatigue loading conditions", *Opt. Las. Eng.*, **47**(3-4), 403-411.
Edwards, A.T. (2000), "Comparison of strain gage and fiber optic sensors on a sting balance in a supersonic wind tunnel", M.Sc. Dissertation, Virginia Polytechnic Institute and State University, Virginai, U.S.A.
Goldston, M., Remennikov, A. and Neaz Sheikh, M. (2016), "Experimental investigation of the behavior of concrete beams reinforced with GFRP bars under static and impact loading", *Eng. Struct.*, **113**, 220-232.
Huang, J. and Newhook, J. (2008), "Structural monitoring system for assessing the long-term behavior of the confederation bridge", *Proceedings of the International Conference of Structures Congress*, Crossing Borders, Vancouver, Canada.
Huang, M., Zhou, Z., Huang, Y. and Ou, J. (2013), "A distributed self-sensing FRP anchor rod with built-in optical fiber sensor", *Measure.*, **46**, 1363-1370.
Jensen, A.E., Havsgard, G.B., Pran, K., Wang, G., Vohra, S.T., Davis, M.A. and Dandrige, A. (2000), "Wet deck slamming experiments with a FRP sandwich panel using a network of 16 fibre optic Bragg grating strain sensors", *Compos. Part B: Eng.*, **31**, 187-198.
Ju, M. and Oh, H. (2015), "Experimental assessment on the flexural bonding performance of concrete beam with GFRP reinforcing bar under repeated loading", *J. Polym. Sci.*, 11.
Ju, M., Oh, H., Lim, J. and Sim, J. (2016), "A modified model for deflection calculation of reinforced concrete beam with deformed GFRP rebar", *J. Polym. Sci.*, 10.
Kara, I.F. (2008), "Flexural performance of FRP-reinforced concrete encased steel composite beams", *Struct. Eng. Mech.*, **59**(4), 775-793.
Kalamkarov, A., Macdonald, D.O., Fitzgerald, S.B. and Georgiades, A.V. (2000), "Reliability assessment of pultruded FRP reinforcements with embedded fiber optic sensors", *Compos. Struct.*, **50**, 69-78.
Kalamkarov, A., Saha, G., Rokkam, S., Newhook, J. and Georgiades, A. (2005), "Strain and deformation monitoring in infrastructure using embedded smart FRP reinforcements", *Compos. Part B: Eng.*, **36**, 455-465.
Lau, K.T., Chan, C.C., Zhou, L.M. and Jin, W. (2001), "Strain monitoring in composite-strengthened concrete structures using optical fibre sensors", *Compos. Part B: Eng.*, **32**, 33-45.
Li, D., Zhou, Z. and Ou, J. (2011), "Development and sensing properties study of FRP-FBG smart stay cable for bridge health monitoring applications", *Measure.*, **44**, 722-729.
Li, D., Zhou, Z. and Ou, J. (2012), "Dynamic behavior monitoring and damage evaluation for arch bridge suspender using GFRP optical fiber Bragg grating sensors", *Opt. Las. Technol.*, **44**(4), 1031-1038.
Li, H.C.H., Herszberg, I., Davis, C.E., Mouritz, A.P. and Galea, S.C. (2006), "Health monitoring of marine composite structural joints using fibre optic sensors", *Compos. Struct.*, **75**, 321-327.
Lu, S. and Xie, H. (2007), "Strengthen and real-time monitoring of RC beam using intelligent CFRP with embedded FBG sensors", *Constr. Build. Mater.*, **21**(9), 1839-1845.
Mao, J., Xu, F., Gao, Q., Liu, S., Jin, W. and Xu, Y. (2016), "A monitoring method based on FBG for concrete corrosion cracking", *Sens.*, **16**, 1093.
Maranan, G., Manalo, A.C., Benmokrane, B., Karunasena, W. and Mendis P. (2015), "Evaluation of the flexural strength and serviceability of geopolymer concrete beams reinforced with glass-fibre-reinforced polymer (GFRP) bars", *Eng. Struct.*, **101**, 529-541.
Thomas, J. and Ramadass, S. (2015), "Design for shear strength of concrete beams longitudinally reinforced with GFRP bars", *Struct. Eng. Mech.*, **53**(1), 41-55.
Moyo, P., Brownjohnb, J.M.W., Sureshc, R. and Tjin, S.C. (2005), "Development of fiber Bragg grating sensors for monitoring civil infrastructure", *Eng. Struct.*, **27**, 1828-1834.
Perrya, M., Yanb, Z., Sunb, Z., Zhang, L., Niewczasa, P. and Johnston, M. (2014), "High stress monitoring of prestressing tendons in nuclear concrete vessels using fibre-optic sensors," *Nucl. Eng. Des.*, **268**, 35-40.
Refai, A.E., Abed, F. and Al-Rahmani, A. (2015), "Structural performance and serviceability of concrete beams reinforced with hybrid (GFRP and steel) bars", *Constr. Build. Mater.*, **96**, 518-529.
Rodrigues, C., Felix, C., Lage, A. and Figueiras, J. (2010), "Development of a long-term monitoring system based on FBG sensors applied to concrete bridges", *Eng. Struct.*, **32**(8), 1993-2002.
Shin, C.S. and Chiang, C.C. (2006), "Fatigue damage monitoring in polymeric composites using multiple fiber bragg gratings", *J. Fatig.*, **28**, 1315-1321.
Takeda, S., Aoki, Y. and Nagao, Y. (2012), "Damage monitoring of CFRP stiffened panels under compressive load using FBG sensors", *Compos. Struct.*, **94**, 813-819.
Tan, G.H., Osborne, N.H. and Brownjohn, J.M. (2008), "Reducing false alerts by improving vibration wire strain gauge data quality using fast fourier transform", *Proceedings of the International Conference on Deep Excavations (ICED)*, Singapore.
Tian, S., Yang, Z., Chen, X. and Xie, Y. (2015), "Damage detection based on static strain responses using FBG in a wind turbine blade", *Sens.*, **15**, 19992-20005.
Tsuda, H. and Lee, J.R. (2007), "Strain and damage monitoring of

CFRP in impact loading using a fiber bragg grating sensor system", *Compos*. *Sci*. *Technol*., **67**, 1353-1361.
Yin, S., Ruffin, P.B. and Yu, F.T.S. (2008), *Fiber Optic Sensors*, CRC Press.
Zhao, X., Gou, J., Song, G. and Ou, J. (2009), "Strain monitoring in glass fiber reinforced composites embedded with carbon nanopaper sheet using fiber bragg grating (FBG) sensors", *Compos*. *Part B*: *Eng*., **40**, 134-140.

CC